Telechelic Poly(ethylene glycol)−POSS Amphiphiles at the Air/Water Interface

Woojin Lee,[†] Suolong Ni,[†] Jianjun Deng,[†,#] Byoung-Suhk Kim,[‡] Sushil K. Satija,[§] Patrick T. Mather,[⊥,‡] and Alan R. Esker*[,†]

Department of Chemistry and Macromolecules and Interfaces Institute, Virginia Tech, Blacksburg, Virginia 24061; Polymer Program and Department of Chemical Engineering, University of Connecticut, Storrs, Connecticut 06269; Center for Neutron Research, National Institute of Standards and Technology, Gaithersburg, Maryland 20899; and Department of Macromolecular Science & Engineering, Case Western Reserve University, Cleveland, Ohio 44106

Received August 9, 2006; Revised Manuscript Received November 7, 2006

ABSTRACT: Combining two non-surface-active building blocks, oligomeric poly(ethylene glycol) (PEG) and a completely hydrophobic polyhedral oligomeric silsesquioxane (POSS) cage, creates amphiphilic telechelic polymers (POSS−PEG−POSS), which exhibit surface activity at the air/water (A/W) interface. POSS moieties serve as the hydrophobic groups for hydrophilic PEG chains of different number-average molar mass (1, 2, 3.4, 8, and 10 kg mol^{-1}). For short PEG chains (1, 2, and 3.4 kg mol^{-1}), insoluble monolayers form, whereas POSS end groups were not sufficiently hydrophobic to keep higher molar mass hydrophilic PEG blocks (8 and 10 kg mol^{-1}) at the A/W interface. Thermodynamic analyses of the 1, 2, and 3.4 kg mol^{-1} POSS−PEG−POSS via surface pressure−area per monomer isotherms indicate that the POSS end groups reside at the A/W interface and that the PEG chains are squeezed into the subphase with increasing surface pressure. This conclusion is supported by X-ray reflectivity studies on Y-type Langmuir−Blodgett multilayer films which reveal a double-layer structure with a double-layer spacing of about 3.52 nm. These findings provide a strategy for producing new surface active species from non-surface-active precursors.

Introduction

Two-dimensional (2D) monolayer studies at the air/water (A/W) interface have attracted interest because of the ability to obtain structural as well as morphological information. Only certain types of molecules, those which exhibit a delicate balance between hydrophilic and hydrophobic contributions to the overall polarity of the molecules, are capable of forming stable monolayers.[1,2] Since Langmuir published his initial study of monolayers of amphiphilic molecules at the A/W interface,[3] numerous materials have been studied in the form of monomolecular films on liquid surfaces (Langmuir films) at constant temperature.[4] Furthermore, some monolayer films can also be transferred onto solid substrates from the water surface through the Langmuir−Blodgett (LB) or Langmuir−Schaefter (LS) techniques. By examining Langmuir films and LB or LS films, it is possible to obtain information about the mechanical, electrical, optical, and chemical properties of oriented molecules at the interface as well as information about structural properties, such as the size and shape of molecules.[5−11]

Poly(ethylene glycol) (PEG) and poly(ethylene oxide) (PEO) are widely studied polymers[12−14] with applications in a variety of technological fields such as drug delivery,[15,16] batteries,[17] and biotechnology.[18] Even though PEG and PEO are completely water-soluble at room temperature, PEO of sufficient molar mass can still form Langmuir monolayers at the A/W interface.[19−22] The amphiphilic nature arises from the ability of the oxygen atom in the ethylene oxide repeating unit (−CH_2CH_2O−) to hydrogen bond with water.[19] The stability of PEO monolayers at the A/W interface depends not only on the surface concentration but also on the molar mass. The lowest reported molar mass for forming stable PEO monolayers at the A/W interface was 18 kg mol^{-1}.[21] In contrast, fully condensed polyhedral oligomeric silsesquioxane (POSS) molecules (Figure 1), such as a closed cage POSS (Figure 1A) (R_8T_8, where T is a silsesquioxane unit and R is alkyl), are nonamphiphilic.[23,24] Given both the theoretical and experimental interest in POSS as a versatile hybrid organic−inorganic material with a core−shell structure,[25−32] and the fact that open cage[33−36] trisilanol−POSS structures (Figure 1B) are amphiphilic ($T_7R_7(OH)_3$, where R is variable), combining POSS with PEG could lead to interesting amphiphiles.

In this study, the combination of PEG oligomers which are too water-soluble to be surface active and a closed cage POSS group which is too hydrophobic to act as a surfactant produces a new type of hybrid amphiphilic telechelic polymer (POSS−PEG−POSS) at the A/W interface possessing interesting insoluble surfactant properties. The advantage of POSS−PEG−POSS molecules (Figure 2) over other telechelic systems is that these materials can serve as building blocks for the construction of hybrid organic−inorganic materials.[37−39] Utilizing results from Brewster angle microscopy (BAM) at the A/W interface and X-ray reflectivity on LB films, the effects of the incorporated hydrophobic POSS on the surface activity and the morphology of POSS−PEG−POSS as well as information about the size and packing of these molecules will be discussed.

Experimental Section

Materials. Five poly(ethylene glycol) (PEG) polymers with nominal monodisperse number-average molar masses of M_n = 1, 2, 3.4, 8, and 10 kg mol^{-1}, designated as PEG_{1K}, PEG_{2K}, $PEG_{3.4K}$, PEG_{8K}, and PEG_{10K}, respectively, were obtained from Aldrich and

* Corresponding author. E-mail: aesker@vt.edu.
[†] Virginia Tech.
[‡] University of Connecticut.
[§] National Institute of Standards and Technology.
[⊥] Case Western Reserve University.
[#] Present address: FPTD SH, Intel Technology Development (Shanghai) Co. Ltd., Pudong Shanghai, 200131, China.

10.1021/ma0618171 CCC: $37.00
Published on Web 01/04/2007

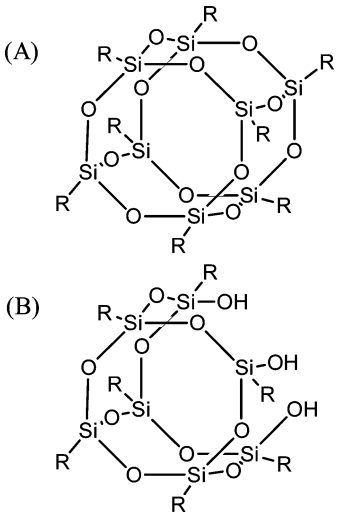

Figure 1. Representative POSS molecules: (A) R_8T_8 and (B) $R_7T_7(OH)_3$. R can be a wide variety of substituents.

purified by twice repeating the process of precipitation into *n*-hexane from chloroform solutions, followed by drying under vacuum overnight.[40] POSS−PEG−POSS samples were synthesized by direct urethane linkages between the hydroxyl end groups of PEG homopolymers and the monoisocyanate group of POSS macromers (isocyanatopropyldimethylsilylcyclohexyl-POSS) provided by the Air Force Research Laboratories, AFRL/PRSM.[37,38] The telechelic polymers are designated here as POSS−PEG_{1K}−POSS, POSS−PEG_{2K}−POSS, POSS−$PEG_{3.4K}$−POSS, POSS−PEG_{8K}−POSS, and POSS−PEG_{10K}−POSS, and their properties are summarized in Table 1. In addition, a high molar mass PEO sample (M_n = 90 kg mol^{-1}, polydispersity index of M_w/M_n = 1.09) was purchased from Polymer Source, Inc., and was used as received.

Surface Pressure−Area Isotherm and BAM Studies. The samples were dissolved in chloroform (HPLC grade, ∼0.5 mg mL^{-1}) without further purification and were spread onto the surface of a standard Langmuir trough (500 cm^2, Nima Technology Ltd. 601 BAM) filled with ultrapure 18.2 MΩ water (Millipore, Milli-Q Gradient A-10) in a Plexiglas box. The compression isotherm studies were carried out at a compression rate of 8 cm^2 min^{-1} and at a constant temperature of 22.5 °C. This compression rate roughly corresponds to 0.04 nm^2 monomer^{-1} min^{-1}. The surface pressure (Π) was recorded by the Wilhelmy plate technique during all isotherm measurements. A completely wetted filter paper plate (contact angle ≈ 0°) was used as the Wilhelmy plate. The variable for the surface concentration was the average area per monomer, *A*. The *A* value was calculated using the calculated average monomer molar mass given in Table 1. Brewster angle microscopy (BAM) studies (MiniBAM, NanoFilm Technologie Ltd., linear resolution ±20 μm) were carried out simultaneously during the isotherm measurements, and the BAM images were recorded using a charge-coupled device camera. The sizes of the BAM images in this paper are 4.8 × 6.4 mm^2. The Langmiur trough, BAM, and Plexiglas box rested on a floating optical table to minimize vibrations.

LB Film Deposition. Silicon substrates [EnCompass Materials Group, Ltd.; dopant: phosphorus, type N, orientation (1,0,0)] were used as LB film substrates for X-ray studies. The substrates were boiled in a 5:1:1 by volume mixture of H_2O:NH_4OH(concentrated):H_2O_2 (30 vol %), for 1.5 h; after rinsing the wafers with Millipore water, the substrates were immersed in a piranha solution [a 70:30 mixture of H_2SO_4 (concentrated):H_2O_2 (30 vol %)] for 0.5 h. The substrates were then rinsed with copious amounts of water, dried with nitrogen, and dipped into a buffered HF acid solution (CMOS Grade, J.T. Baker) for 5 min followed by a brief dip into a buffered NH_4F solution (CMOS Grade, J.T. Baker). The substrates were again rinsed with water and dried with nitrogen. The H_2O_2, H_2SO_4, and NH_4OH used in the cleaning process were obtained from EM Science, VWR International, and Fisher Scientific, respectively.

Ultrathin LB films were obtained for POSS−PEG_{1K}−POSS using a commercial LB trough (KSV 2000) by Y-type deposition.[11] The compression rate for approaching the target Π = 25 mN m^{-1} was 10 mm min^{-1}, as was the maximum forward and reverse rate of the barriers during the dipping process to maintain a constant target Π. The dipping rates were 10 mm min^{-1} for both the up and down strokes, and a 2 min delay time was used between each dipping cycle.

Specular X-ray Reflectivity. The specular X-ray reflectivity measurements were performed at the NIST Center for Neutron Research using Cu Kα radiation with a wavelength of 0.154 nm on a Bruker AXS-D8 Advance diffractometer. The thicknesses of the films were obtained by plotting the refraction-corrected successive minima vs minima index as described by Thompson et al.[41] Roughnesses of both the film and the substrate were obtained by fitting the experimental profiles with theoretical curves in Microsoft Excel.[42,43]

Results and Discussion

Compression Isotherm Studies of PEG vs POSS−PEG−POSS. The combination of two nonsurfactants such as water-soluble PEG oligomers and completely hydrophobic POSS cages yields telechelic polymers with surface properties that are strongly molar mass dependent, as our results reveal below.

(1) PEG_{1K} vs POSS−PEG_{1K}−POSS. Figure 3 shows Π−*A* isotherms of PEG_{1K} and POSS−PEG_{1K}−POSS. It is obvious that PEG_{1K} exhibits almost no surface activity, whereas the POSS−PEG_{1K}−POSS analog forms insoluble films. Here it should be noted that the isotherm for PEG_{1K} shows an increase in Π during a dynamic compression experiment. However, after the cessation of compression, Π decays to zero, indicating that the PEG itself is incapable of forming an insoluble monolayer. For POSS−PEG_{1K}−POSS, at very large molecular areas, *A*, the monolayer is in a gaslike state (G). Upon film compression, the coexistence of G and a liquidlike film is expected, even though we are unable to resolve this coexistence by BAM. As the lift-off *A* value ($A_{lift-off}$ ≈ 0.20 nm^2 monomer^{-1}) is approached, Π begins to increase. For the expanded monolayer region, 0.13 < *A* < 0.20 nm^2 monomer^{-1}, the surface pressure starts to rise slowly like high molar mass PEO and has a compressibility that is consistent with a liquid-expanded (LE) phase. Further compression of the monolayer (0.11 < *A* < 0.13 nm^2 monomer^{-1}) leads to the formation of a more condensed (LC) phase; however, on the basis of BAM images, the film remains homogeneous. In the LC region, Π rises dramatically with small changes in *A* showing the effect of the less compressible POSS groups at the A/W interface. By extrapolating the steepest portion of the isotherm back to the *x*-axis (Π = 0), one obtains a limiting cross-sectional area, A_0 ≈ 0.13 nm^2 monomer^{-1}. The A_0 value of 0.13 nm^2 monomer^{-1} is interesting if one considers that POSS−PEG_{1K}−POSS is composed of 24 repeating units (22 EO and 2 POSS). Hence, A_0 can also be defined as ≈1.62 nm^2 POSS^{-1}. This value is close to the reported collapse area for trisilanolcyclohexyl-POSS.[34] As all films are still homogeneous in BAM images, it appears that the region from 0.11 < *A* < 0.13 nm^2 monomer^{-1} corresponds to a POSS monolayer with all PEG segments squeezed into the subphase. Hence, the sharp rise in Π apparently reflects the rigidity of the POSS units of POSS−PEG_{1K}−POSS. For compression to *A* < 0.11 nm^2 monomer^{-1} (Π > 30 mN m^{-1}), there is a change in slope on the Π−*A* isotherm in Figure 3 that we interpret as the formation of multilayer structures. The evidence for this conclusion comes from heterogeneous BAM images in this region (BAM image in Figure 3) showing rigid and collapsed domains.[8,44,45] The images are consistent with POSS being squeezed out of the

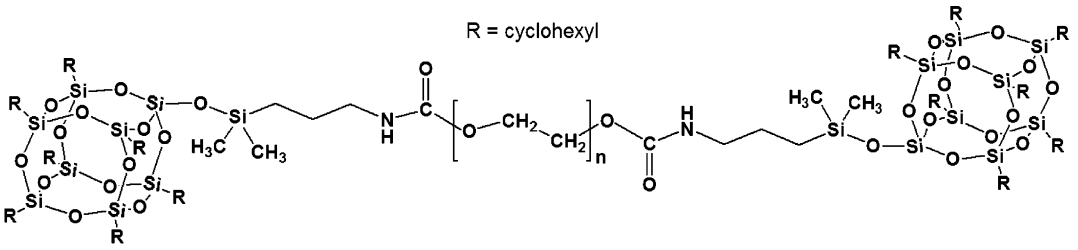

Figure 2. POSS−PEG−POSS molecules.[37−39] R is a cyclohexyl group for these studies.

Table 1. Molar Mass Characteristics of the POSS−PEG−POSS[37,38]

	calculated[b]		NMR			GPC	
$POSS_x-EO_y-POSS_x$[a] $x/y/x$ (designation)	monomer M_n[c]	polymer M_n[c]	M_n[c]	[POSS]/[PEG]	wt % of POSS	M_w[c]	M_w/M_n
1/22/1 (POSS−PEG_{1K}−POSS)	137.46	3300	3470	2.15	68.1	3470	1.02
1/44/1 (POSS−PEG_{2K}−POSS)	92.79	4300	4480	2.16	52.7	4480	1.08
1/74/1 (POSS−$PEG_{3.4K}$−POSS)	73.55	5700	5730	2.03	40.7	5730	1.02
1/174/1 (POSS−PEG_{8K}−POSS)	56.79	10300	10200	1.94	23.6	10230	1.03
1/217/1 (POSS−PEG_{10K}−POSS)	54.29	12300	12100	1.86	19.8	12140	1.04

[a] Nominal number of repeating units (designated as monomers) for the ethylene oxide (EO) and the end groups (POSS). Text in parentheses are the designation of telechelic polymers prepared from PEG with different molar masses. [b] Calculated values assume the POSS−EO−POSS ratios are correct and assumes a POSS unit counts the same as an EO unit for monomer calculations. [c] All molar mass values have the units of g mol^{-1}.

monolayer into multilayer structures (squeezed out into air rather than into the subphase). The schematic depiction appearing on the isotherm in Figure 3 provides a qualitative description of how we believe the monolayer packs in the region from 0.11 $< A <$ 0.13 nm^2 $monomer^{-1}$. In essence, like another telechelic polymer where hydrophobic alkyl end groups anchor PEG at the interface,[46] the two POSS groups anchor the molecule to the A/W interface, thereby preventing the dissolution of the PEG chain. The key difference is that POSS groups allow us to obtain a surfactant with a much shorter PEG.

(2) PEG_{2K} vs POSS−PEG_{2K}−POSS. Figure 4 shows a plot of $\Pi-A$ isotherms of PEG_{2K} and POSS−PEG_{2K}−POSS. Comparing PEG_{2K} with POSS−PEG_{2K}−POSS reveals differences from the analogous PEG_{1K} systems. Similar to PEG_{1K}, PEG_{2K} shows limited surface activity because of its high water solubility. As noted for PEG_{1K}, transient Π values during the dynamic compression experiment are not indicative of insoluble film formation, and Π also falls to zero when compression ceases for PEG_{2K}. Much like POSS−PEG_{1K}−POSS, POSS−PEG_{2K}−POSS forms stable insoluble monolayers. At low concentrations of POSS−PEG_{2K}−POSS ($\Pi \approx 0$ mN m^{-1}), such as $A >$ 0.20 nm^2 $monomer^{-1}$, the film likely exists in a G phase like POSS−PEG_{1K}−POSS. The most obvious difference between POSS−PEG_{1K}−POSS and POSS−PEG_{2K}−POSS is the decrease in $A_{lift-off}$ from 0.20 to 0.10 nm^2 $monomer^{-1}$, respectively. This factor of 2 decrease is an exact consequence of doubling the molar mass of the PEG segment. As a result, the LE (0.07 $< A <$ 0.20 nm^2 $monomer^{-1}$) and LC (0.05 $< A <$ 0.07 nm^2 $monomer^{-1}$) phases are shifted to smaller A values for POSS−PEG_{2K}−POSS. These shifts are highlighted in the inset of Figure 4. Similarly, A_0 decreases to $\approx$0.07 nm^2 $monomer^{-1}$. Like POSS−PEG_{1K}−POSS, this value can also be expressed as $\approx$1.58 nm^2 $POSS^{-1}$, a number that is consistent with a POSS monolayer at the surface and PEG chains looping into the subphase. Furthermore, there is also a slope change around $\Pi \approx 30$ mN m^{-1} leading to film heterogeneity as seen by BAM (Figure 4).

(3) $PEG_{3.4K}$ vs POSS−$PEG_{3.4K}$−POSS. Figure S1 (Supporting Information) shows $\Pi-A$ isotherms for $PEG_{3.4K}$ and POSS−$PEG_{3.4K}$−POSS. Like POSS−PEG_{2K}−POSS, the POSS−$PEG_{3.4K}$−POSS $\Pi-A$ isotherm features shift to smaller A values ($A_{lift-off} \approx$ 0.06 nm^2 $monomer^{-1}$, 0.04 $< A$ (LE) $<$ 0.06 nm^2 $monomer^{-1}$, and 0.03 $< A$ (LC) $<$ 0.04 nm^2 $monomer^{-1}$). These shifts mainly arise from the molar mass of the PEG segment

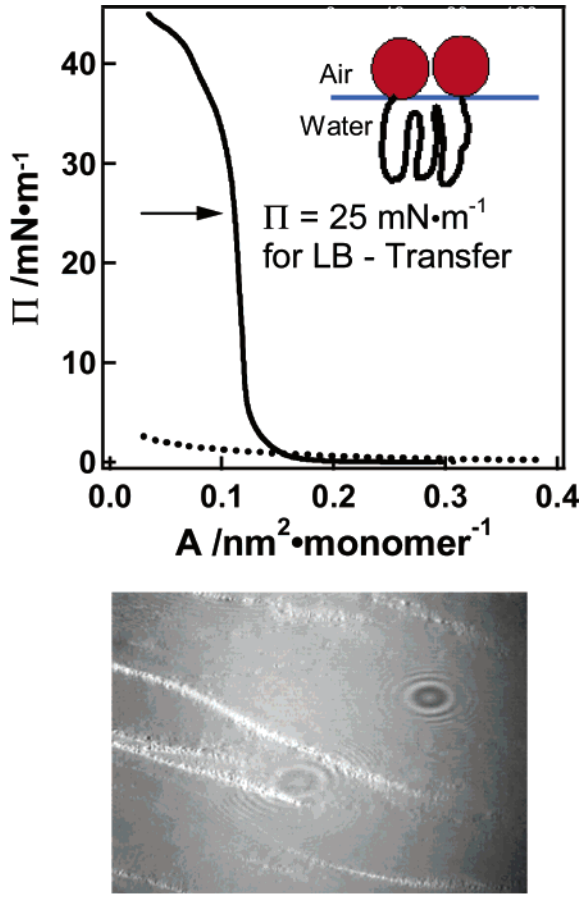

Figure 3. $\Pi-A$ isotherms of PEG_{1K} (dotted line) and POSS−PEG_{1K}−POSS (solid line) with a compression rate of 0.04 nm^2 $monomer^{-1}$ min^{-1} at $T = 22.5$ °C. The schematic on the isotherm corresponds to the presumed packing at the A/W interface for 0.11 $< A <$ 0.13 nm^2 $monomer^{-1}$. The circles correspond to POSS groups and the thick wormlike lines indicate PEG_{1K} in the schematic. The arrow indicates the Π value for LB-film formation. The 4.8 × 6.4 mm^2 BAM image was taken at $A = 0.04$ nm^2 $monomer^{-1}$, showing representative heterogeneity that appears in the film for compression to $\Pi >$ 30 mN m^{-1}. For the BAM image, compression was symmetric from the top and bottom of the image.

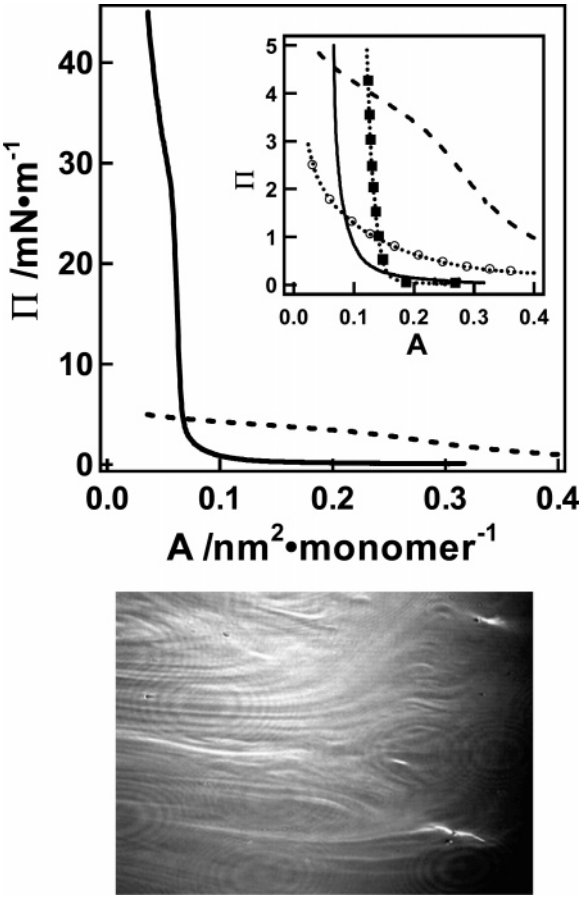

Figure 4. Π−*A* isotherms of PEG_{2K} (dashed line) and POSS−PEG_{2K}−POSS (solid line) with a compression rate of 0.04 nm^2 $monomer^{-1}$ min^{-1} at $T = 22.5$ °C. The inset highlights $A_{lift-off}$ for POSS−PEG_{1K}−POSS (■), PEG_{1K} (○), POSS−PEG_{2K}−POSS (solid line), and PEG_{2K} (dashed line). The 4.8 × 6.4 mm^2 BAM image was taken at $A = 0.03$ nm^2 $monomer^{-1}$ showing representative heterogeneity that appears in the film for compression to Π > 30 mN m^{-1}. For the BAM image, the film was symmetrically compressed from the top and bottom of the image.

with an attendant shift of $A_0 \approx 1.4$ nm^2 $POSS^{-1}$. As this value is smaller than the POSS−PEG_{1K}−POSS and POSS−PEG_{2K}−POSS system, some POSS units may be pulled into the subphase by the larger PEG segment. Nonetheless, the majority of the POSS groups are believed to form a monolayer with looped PEG in the subphase. Similar to POSS−PEG_{1K}−POSS and POSS−PEG_{2K}−POSS, POSS−$PEG_{3.4K}$−POSS isotherms exhibit a changing slope at Π ≈ 30 mN m^{-1}, leading to multilayer formation. One significant difference is the shape of the transient (constant compression) isotherm of $PEG_{3.4K}$. As seen in Figure S1, the $PEG_{3.4K}$ isotherm has a shape that is similar to high molar mass PEO even though Π drops to zero once compression stops.

(4) PEG_{8K} and PEG_{10K} vs POSS−PEG_{8K}−POSS and POSS−PEG_{10K}−POSS. Inspection of Figure 5, with compression isotherm data for PEG_{8K} and PEG_{10K}, reveals shapes and transition features that are similar to high molar mass PEO. However, the PEG_{8K} and PEG_{10K} samples, like the lower molar mass PEG samples, fail to form stable monolayers. Once compression of the monolayer ceases, Π decays to zero with time. Interestingly, the POSS−PEG_{8K}−POSS and POSS−PEG_{10K}−POSS samples suffer from the same problem as PEG_{8K} and PEG_{10K}. Upon the cessation of compression, Π falls toward zero with time for POSS−PEG_{8K}−POSS and POSS−PEG_{10K}−POSS. In this respect, the transient Π−*A* isotherms obtained during constant compression for POSS−PEG_{8K}−POSS and

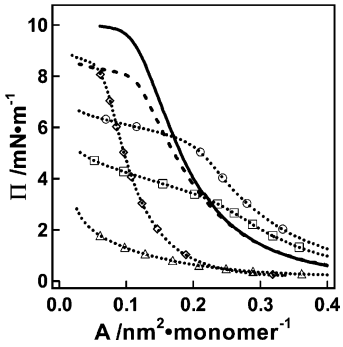

Figure 5. Π−*A* isotherms of PEO_{90K} (solid line), PEG_{10K} (◊), PEG_{8K} (dashed line), $PEG_{3.4K}$ (○), PEG_{2K} (□), and PEG_{1K} (Δ) obtained at $T = 22.5$ °C during compression at a fixed rate. Only the PEO_{90K} sample forms a stable Langmuir film.

POSS−PEG_{10K}−POSS are more similar to PEG_{8K} and PEG_{10K} (Figure S2, Supporting Information) than the lower molar mass systems. Hence, the conclusion is clear. POSS end groups are insufficiently hydrophobic to keep intermediate molar mass PEO at the A/W interface (here intermediate molar mass represents the range between roughly 4 and 18 kg mol^{-1}, the lowest reported molar mass for stable PEO Langmuir film formation).[21] In light of a recent report on solution viscosity behavior of POSS−PEG_{10K}−POSS, it appears that micelles may form in solution.[39]

Isotherm Stability. As noted throughout the discussion above, monolayer stability is a principal concern for the POSS−PEG−POSS system. The stability of various films can be probed by looking at ΔΠ vs time at constant *A*. For POSS−PEG−POSS molecules with low molar mass PEG, such as POSS−PEG_{1K}−POSS, POSS−PEG_{2K}−POSS, and POSS−$PEG_{3.4K}$−POSS, the films are moderately stable. The relaxation experiments show that the pressure drops to values of Π ≈ 26, 25, and 17 mN m^{-1} after compression to high Π values (Π > 45 mN m^{-1}) for POSS−PEG_{1K}−POSS, POSS−PEG_{2K}−POSS, and POSS−$PEG_{3.4K}$−POSS, respectively. In contrast, POSS−PEG_{8K}−POSS and POSS−PEG_{10K}−POSS relax to a surface pressure of nearly zero. This relaxation in Π does not occur for high molar mass PEO. The fact that the POSS−PEG−POSS polymers for 8 and 10 kg mol^{-1} PEG fail to remain at the surface reflects the fact that POSS is insufficiently hydrophobic to anchor the molecules to the A/W interface as previously suggested in the discussion. With increasing molar mass of the PEG segments, there is a constant shift to smaller *A* values reflecting the falling weight percentage of POSS in the POSS−PEG−POSS polymers. Since the average number of PEG segments for POSS−PEG_{2K}−POSS and POSS−$PEG_{3.4K}$−POSS are 2 and 3.4 times as great as those of POSS−PEG_{1K}−POSS, the cross-sectional monomer areas (A_0) of POSS−PEG_{2K}−POSS and POSS−$PEG_{3.4K}$−POSS are approximately $^1/_2$ and $^1/_3$ the value of POSS−PEG_{1K}−POSS (Figure S3, Supporting Information).

In addition, Figure S3 shows a comparison of Π−*A* isotherms for POSS−PEG−POSS molecules that form stable spread films. The *A* values corresponding to the LE phase become progressively smaller with increasing molar mass. Similarly, *A* values for the formation of an LC region also shift to smaller *A* as the wt % of PEG increases. The slope of the LC phase appears to be steeper as the wt % of PEG increases; however, a better comparison is the static elasticity, $\epsilon_s = -A(\{\partial\Pi\}/\{\partial A\})_T$, which actually shows a decrease in the maximum ϵ_s (Figure S4, Supporting Information). The large ϵ_s values (ϵ_s > 100 mN m^{-1}) observed in the LC regime for the 1, 2, and 3.4 kg mol^{-1} POSS−PEG−POSS, and the trend of decreasing ϵ_s with

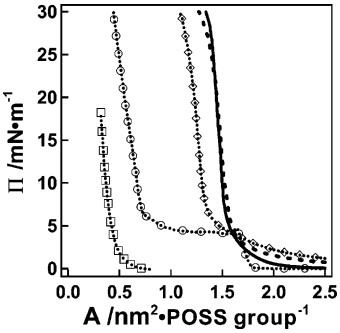

Figure 6. Π−*A* isotherms of POSS−PEG_{1K}−POSS (solid line), POSS−PEG_{2K}−POSS (dashed line), POSS−$PEG_{3.4K}$−POSS (◇), $Cy_7T_7(OH)_3$ (○), and Cy_8T_8 (□) as a function of area per POSS group.

increasing PEG molar mass for the POSS−PEG−POSS series provides a strong indication that the behavior is controlled by the surface density of the POSS end groups. This supposition will be explored in the next section.

POSS−PEG−POSS Behavior as a Function of POSS Surface Density. Figure 6 shows Π−*A* isotherms of POSS−PEG_{1K}−POSS, POSS−PEG_{2K}−POSS, and POSS−$PEG_{3.4K}$−POSS as a function of the surface area per POSS end group, A_{POSS}. For comparison, Figure 6 also contains isotherms for trisilanolcyclohexyl-POSS, $Cy_7T_7(OH)_3$, and octacyclohexyl-POSS, Cy_8T_8. It is obvious from Figure 6 that Cy_8T_8 molecules form multilayers even at low surface pressure (Π ≈ 0 mN m^{-1}); thus, it is impossible to estimate a reasonable area per POSS molecule from the figure. This behavior is expected on the basis of previously reported data for octaisobutyl-POSS[23,24] and the completely hydrophobic character of Cy_8T_8. On the other hand, it is possible to estimate the area each cyclohexyl-substituted POSS cage occupies from $Cy_7T_7(OH)_3$ since these molecules form stable monolayers and feature nearly identical structures. The A_0 value for the $Cy_7T_7(OH)_3$ molecule is ≈1.81 nm^2 $POSS^{-1}$, and the area at the onset of the collapse transition is ≈1.64 nm^2 $POSS^{-1}$.[34] Looking at Figure 6, it is interesting to note that the *A* value for the onset of the LC phase for POSS−PEG_{1K}−POSS and POSS−PEG_{2K}−POSS (A_0 ≈ 1.6 nm^2 $POSS^{-1}$) corresponds very well with the collapse area of $Cy_7T_7(OH)_3$. Hence, a reasonable conclusion would be that PEG is squeezed into the subphase at the start of the LC phase (Π > 5 mN m^{-1}), and a POSS "monolayer" exists for POSS−PEG_{1K}−POSS and POSS−PEG_{2K}−POSS until these monolayers collapse during constant compression experiments around Π ≈ 30 mN m^{-1}. It is interesting to note that the LC phase for POSS−$PEG_{3.4K}$−POSS forms at smaller *A* values (≈ 1.4 nm^2 $POSS^{-1}$). This feature is consistent with the previously noted increase in solubility for POSS−PEG−POSS with increasing PEG molar mass. As seen in Figure S5 (Supporting Information), the trend of smaller *A* for increasing PEG molar mass for POSS−PEG−POSS does not continue for POSS−PEG_{8K}−POSS and POSS−PEG_{10K}−POSS during constant compression experiments. For these two systems the area per POSS group is much larger as the PEG component dominates the constant compression isotherm. Nonetheless, the POSS−PEG_{8K}−POSS and POSS−PEG_{10K}−POSS isotherms in Figure S5 are only transient as the molecules do not form insoluble monolayers.

X-ray Reflectivity Results for Tel-POSS−PEG1K. Importantly, the careful balance between the hydrophobic POSS and the hydrophilic PEG_{1K} allows for the formation of LB multilayer films by Y-type deposition. In contrast, higher molar mass PEG telechelics are too hydrophilic to form Y-type LB multilayer films. Figure 7 shows X-ray reflectivity profiles for a series of

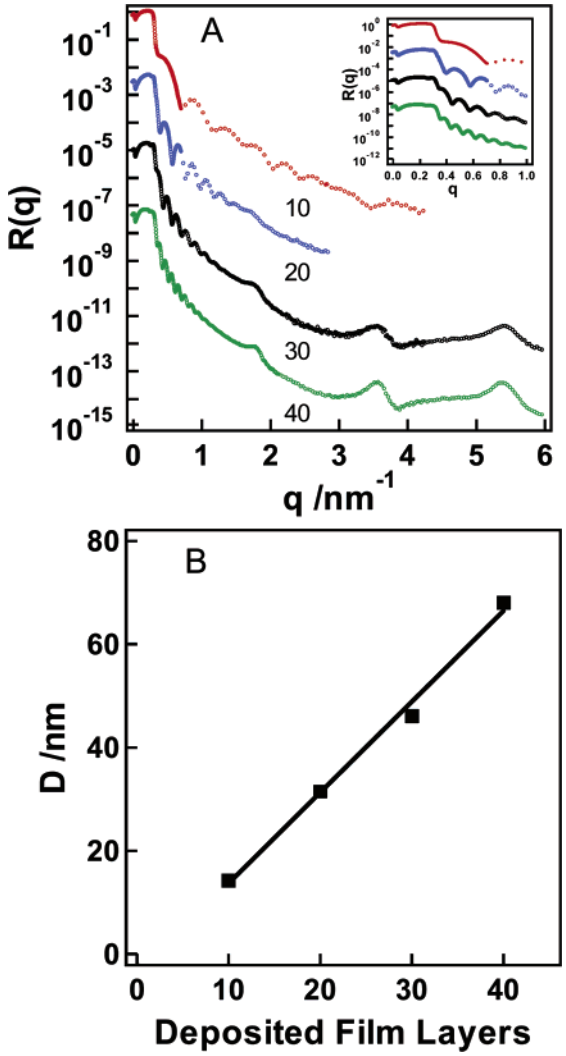

Figure 7. (A) X-ray reflectivity profiles from 10-, 20-, 30-, and 40-layer LB-films as indicated on the graph for POSS−PEG_{1K}−POSS deposited at Π = 25 mN m^{-1} and *T* = 22.5 °C. The reflectivity values of the 20-, 30-, and 40-layer films are shifted by 2, 5, and 7 decades, respectively, for clarity. The inset highlights how the Kiessig fringe spacing depends on film thickness. (B) The total film thickness vs the number of deposited film layers. The slope of *d* = 1.76 ± 0.09 nm provides the thickness of a POSS−PEG_{1K}−POSS monolayer.

POSS−PEG_{1K}−POSS LB films on silicon substrates. The total numbers of transferred layers for the LB films are 10, 20, 30, and 40 layers. Because of the thickness and low surface roughness of each specimen, the reflectivity profiles exhibit periodic oscillations, Kiessig fringes, whose spacings correspond to the total film thickness through Bragg's law. By analyzing the Kiessig fringe spacings,[41] it is possible to generate Figure 7B, a plot of the total thickness (*D*) vs the number of transferred layers. The slope of Figure 7B yields the thickness of a POSS−PEG_{1K}-POSS monolayer in the LB-film, *d* = 1.76 ± 0.09 nm. Slightly less than quantitative transfer ratios on the first few dipping cycles leads to a nonzero (negative) intercept. This feature provides justification to use the slope of Figure 7B rather than the total film thickness divided by the number of transferred layers, as a better indicator of layer thickness. Another significant feature of the 30- and 40-layer films is the Bragg peaks observed at 1.78, 3.56, and 5.45 nm^{-1}. The observation of Bragg peaks in the LB films arises from the presence of a double-layer structure with a sufficiently large difference in electron density between the hydrophilic head groups and the hydrophobic tails. In this case, the hydrophobic POSS end

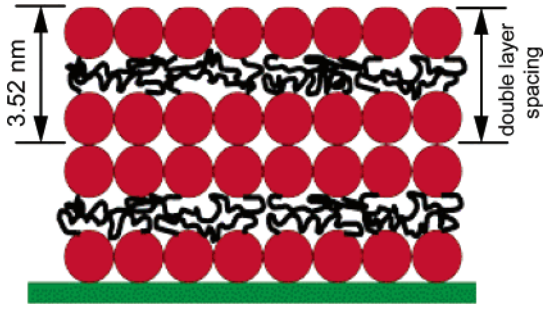

Figure 8. A schematic depiction of a POSS−PEG_{1K}−POSS LB-film (four layers) obtained by Y-type deposition at $\Pi = 25$ mN m^{-1} and room temperature ($T = 22.5$ °C). The double-layer spacing is ≈3.52 nm. Spheres represent POSS units while wormlike chains represent PEG segments.

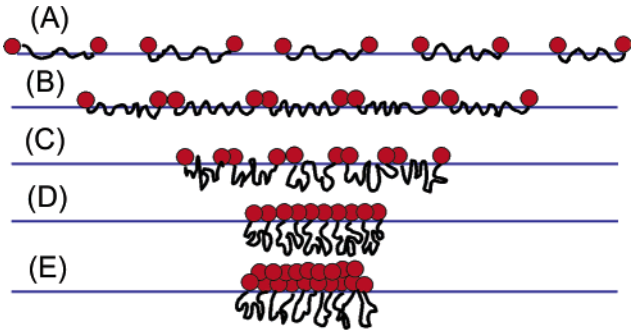

Figure 9. Proposed packing model for POSS−PEG_{1K}−POSS molecules based on Π−*A* isotherm, BAM, and X-ray reflectivity studies. Spheres represent POSS units while wormlike chains represent PEG segments. (A) $\Pi \approx 0$ mN m^{-1}: the molecules are dispersed at the A/W interface (G or G/LE films). (B) $\Pi \approx 1$ mN m^{-1}: compression allows the molecules to form a LE phase. (C) $1 < \Pi < 5$ mN m^{-1}: further compression leads to a brushlike conformation for the PEG chains. (D) $5 < \Pi < 30$ mN m^{-1}: a LC film of closely packed POSS units and PEG loops. (E) $\Pi > 30$ mN m^{-1}: collapse of POSS units into mutilayer domains.

groups are concentrated into layers with higher electron density than the hydrophilic PEG-rich layers.

Packing in LB−Films and at the A/W Interface. The Bragg peak spacing in Figure 7 means that the double-layer spacing for POSS−PEG_{1K}−POSS LB films is ≈3.52 nm, as depicted schematically in Figure 8. This value is consistent with the slope-based analysis of the layer thickness in Figure 7B. As the double layer has a spacing of 3.52 nm, and if one assumes that the PEG layer has an amorphous PEG density (1.13 g cm^{-3}), the calculated diameter of each cyclohexyl-substituted POSS cage must be ≈1.24 nm. This "diameter" is smaller than simple AM1 calculations (diameter ≈ 1.45 nm) but larger than the reported thickness of a trisilanolphenyl-POSS LB layer (0.84 nm).[47] Using a smaller POSS thickness necessarily leads to a thicker, i.e., less dense PEG layer. Nonetheless, at the A/W interface, the PEG layer should swell and is expected to have a thickness on the order of ≈2 nm at the A/W interface based on neutron reflectivity studies for higher molar mass PEO samples.[48]

On the basis of the structural information obtained from the LB films and previously published neutron reflectivity studies,[48] a model for POSS−PEG_{1K}−POSS samples at the A/W interface is proposed in Figure 9. At $\Pi \approx 0$ mN m^{-1}, the molecules are dispersed at the surface. PEG chains can stay at the air interface or loop into the subphase (Figure 9A). As compression proceeds, the molecules start to interact ($\Pi \approx 1$ mN m^{-1}), and osmotic forces comparable to those in high molar mass PEO monolayers are present (Figure 9B). With further compression ($1 < \Pi < 5$ mN m^{-1}), PEG segments will preferentially loop into the subphase (Figure 9C) with dissolution being hindered by the POSS anchors. For $\Pi > 5$ mN m^{-1}direct interactions between POSS end groups are expected, resulting in rigid (high modulus) films and the formation of a structure (Figure 9D) that is comparable to the POSS−PEG_{1K}−POSS conformation observed in the LB film (Figure 8). Further compression to $\Pi > 30$ mN m^{-1} leads to the collapse of the POSS−PEG_{1K}−POSS monolayer into multilayer aggregates (Figure 9E) on the basis of the BAM image in Figure 3.

Conclusions

In this study, two nonamphiphilic species, water-soluble oligomeric PEG and an insoluble hydrophobic closed cage POSS unit, are combined to produce amphiphilic POSS−PEG−POSS molecules. Π−*A* isotherm and BAM measurements for amphiphilic POSS−PEG−POSS with 1, 2, and 3.4 kg mol^{-1} PEG confirm dramatically different behavior from isotherm studies of 1, 2, and 3.4 kg mol^{-1} oligomeric PEG molecules at the A/W interface. The balance of the hydrophilic and hydrophobic moieties is such that it is even possible to make Y-type LB multilayer films for POSS−PEG_{1K}−POSS. X-ray reflectivity shows the LB films are comprised of 1.76 nm layers with a resolvable double-layer structure that arises from segregated hydrophobic POSS and hydrophilic PEG moieties. This study clearly demonstrates the feasibility of creating hybrid organic−inorganic surfactants from nonamphiphilic building blocks and using these principles to create nanostructured materials and coatings.

Acknowledgment. A.R.E. gratefully acknowledges financial support of this work coming from the 3M Untenured Faculty Award Program, the Virginia Tech Aspires Program, the Thomas F. Jeffress and Kate Miller Jeffress Memorial Trust (J-553), and the National Science Foundation (CHE-0239633). P.T.M. gratefully acknowledges support from AFOSR/NL (FA9550-05-1-0142).

Supporting Information Available: Additional isotherms and static elasticity data. This material is available free of charge via the Internet at http://pubs.acs.org.

References and Notes

(1) Gaines, G. L. *Insoluble Monolayers at Liquid-Gas Interfaces*; John Wiley & Sons: New York, 1966.
(2) Lenk, T. J.; Lee, D. H. T.; Koberstein, J. T. *Langmuir* **1994**, *10*, 1857.
(3) Langmuir, I. *J. Am. Chem. Soc.* **1917**, *39*, 1848.
(4) Kawaguchi, M. *Prog. Polym. Sci.* **1993**, *18*, 341.
(5) Knobler, C. M.; Desai, R. C. *Annu. Rev. Phys. Chem.* **1992**, *43*, 207.
(6) Kawaguchi, M.; Sauer, B. B.; Yu, H. *Macromolecules* **1989**, *22*, 1735.
(7) Granick, S.; Clarson, S. J.; Formoy, T. R.; Semlyen, J. A. *Polymer* **1985**, *26*, 925.
(8) Kim, Y.; Pyun, J.; Frechet, J. M. J.; Hawker, C. J.; Frank, C. W. *Langmuir* **2005**, *21*, 10444.
(9) Wegner, G. *Macromol. Chem. Phys.* **2003**, *204*, 347.
(10) Kaganer, V. M.; Möhwald, H.; Dutta, P. *Rev. Mod. Phys.* **1999**, *71*, 779.
(11) Ulman, A. *An Introduction to Ultrathin Organic Films*; Academic Press: San Diego, 1998.
(12) Goncalves da Silva, A. M.; Simoes Gamboa, A. L.; Martinho, J. M. G. *Langmuir* **1998**, *14*, 5327.
(13) Peace, S. K.; Richards, R. W.; Kiff, F. T.; Webster, J. R. P.; Williams, N. *Polymer* **1998**, *40*, 207.
(14) Xu, Z.; Holland, N. B.; Marchant, R. E. *Langmuir* **2001**, *17*, 377.
(15) Lasic, D. D. *Nature (London)* **1996**, *380*, 561.
(16) Jo, Y. S.; Kim, M. C.; Kim, D. K.; Kim, C. J.; Jeong, Y. K.; Kim, K. J.; Muhammed, M. *Nanotechnology* **2004**, *15*, 1186.
(17) Zaghib, K.; Charest, P.; Guerfi, A.; Shim, J.; Perrier, M.; Striebel, K. *J. Power Sources* **2004**, *134*, 124.
(18) Aktas, Y.; Yemisci, M.; Andrieux, K.; Gursoy, R. N.; Alonso, M. J.; Fernandez-Megia, E.; Novoa-Carballal, R.; Quinoa, E.; Riguera, R.;

Sargon, M. F.; Celik, H. H.; Demir, A. S.; Hincal, A. A.; Dalkara, T.; Capan, Y.; Couvreur, P. *Bioconjugate Chem.* **2005**, *16*, 1503.
(19) Shuler, R. L.; Zisman, W. A. *J. Phys. Chem.* **1970**, *74*, 1523.
(20) Kawaguchi, M.; Komatsu, S.; Matsuzumi, M.; Takahashi, A. *J. Colloid Interface Sci.* **1984**, *102*, 356.
(21) Sauer, B. B.; Yu, H. *Macromolecules* **1989**, *22*, 786.
(22) Kuzmenka, D. J.; Granick, S. *Macromolecules* **1988**, *21*, 779.
(23) Deng, J. J.; Polidan, J. T.; Hottle, J. R.; Farmer-Creely, C. E.; Viers, B. D.; Esker, A. R. *J. Am. Chem. Soc.* **2002**, *124*, 15194.
(24) Hottle, J. R.; Deng, J. J.; Kim, H.-J.; Farmer-Creely, C. E.; Viers, B. D.; Esker, A. R. *Langmuir* **2005**, *21*, 2250.
(25) Gonzalez, R. I.; Phillips, S. H.; Hoflund, G. B. *J. Spacecraft Rockets* **2000**, *37*, 463.
(26) Knischka, R.; Dietsche, F.; Hanselmann, R.; Frey, H.; Mülhaupt, R.; Lutz, P. J. *Langmuir* **1999**, *15*, 4752.
(27) Tsuchida, A.; Bolln, C.; Sernetz, F. G.; Frey, H.; Mülhaupt, R. *Macromolecules* **1997**, *30*, 2818.
(28) Kopesky, E. T.; Haddad, T. S.; McKinley, G. H.; Cohen, R. E. *Polymer* **2005**, *46*, 4743.
(29) Sulaiman, S.; Brick, C. M.; De Sana, C. M.; Katzenstein, J. M.; Laine, R. M.; Basheer, R. A. *Macromolecules* **2006**, *39*, 5167.
(30) Zheng, L.; Farris, R. J.; Coughlin, E. B. *Macromolecules* **2001**, *34*, 8034.
(31) Liang, K. W.; Toghiani, H.; Li, G. Z.; Pittman, C. U. *J. Polym. Sci., Part A: Polym. Chem.* **2005**, *43*, 3887.
(32) Yoon, K. H.; Polk, M. B.; Park, J. H.; Min, B. G.; Schiraldi, D. A. *Polym. Int.* **2005**, *54*, 47.
(33) Hottle, J. R.; Kim, H.-J.; Deng, J. J.; Farmer-Creely, C. E.; Viers, B. D.; Esker, A. R. *Macromolecules* **2004**, *37*, 4900.
(34) Deng, J. J.; Farmer-Creely, C. E.; Viers, B. D.; Esker, A. R. *Langmuir* **2004**, *20*, 2527.
(35) Deng, J. J.; Viers, B. D.; Esker, A. R.; Anseth, J. W.; Fuller, G. G. *Langmuir* **2005**, *21*, 2375.
(36) Kim, H.-J.; Deng, J. J.; Hoyt Lalli, J.; Riffle, J. S.; Viers, B. D.; Esker, A. R. *Langmuir* **2005**, *21*, 1908.
(37) Kim, B.-S.; Mather, P. T. *Macromolecules* **2002**, *35*, 8378.
(38) Mather, P. T.; Kim, B.-S.; Ge, Q.; Liu, C. US Patent 7,067,606 B2, 2006.
(39) Kim, B.-S.; Mather, P. T. *Polymer* **2006**, *47*, 6202.
(40) Certain commercial materials and instruments are identified in this paper to adequately specify the experimental procedure. In no case does such identification imply recommendation or endorsement by the National Institute of Standards and Technology, nor does it imply that materials or equipment identified are necessarily the best available for the purposes.
(41) Thompson, C.; Saraf, R. F.; Jordan-Sweet, J. L. *Langmuir* **1997**, *13*, 7135.
(42) Welp, K. A.; Co, C. C.; Wool, R. P. *Neutron Res.* **1999**, *8*, 37.
(43) Esker, A. R.; Grull, H; Satija, S. K.; Han, C. C. *J. Polym. Sci., Part B: Polym. Phys.* **2004**, *42*, 3248.
(44) Lipp, M. M.; Lee, K. Y. C.; Waring, A.; Zasadzinski, J. A. *Biophys. J.* **1997**, *72*, 2783.
(45) Buzin, A. I.; Godovsky, Yu. K.; Makarova, N. N.; Fang, J.; Wang, X.; Knobler, C. M. *J. Phys. Chem. B* **1999**, *103*, 11372.
(46) Barentin, C.; Muller, P.; Joanny, J. F. *Macromolecules* **1998**, *31*, 2198.
(47) Karabiyik, U.; Esker, A. R. *Proc. Annu. Meet. Adhes. Soc.* **2005**, *28*, 253.
(48) Henderson, J. A.; Richards, R. W.; Penfold, J.; Thomas, R. K.; Lu, J. R. *Macromolecules* **1993**, *26*, 4591.

MA0618171